

# **Analyst**

## Probe Oscillation Control in Tapping-mode Scanning Probe Electrospray Ionization for Stabilization of Mass Spectrometry Imaging

Journal:	Analyst
Manuscript ID	AN-ART-05-2024-000712.R1
Article Type:	Paper
Date Submitted by the Author:	17-Jun-2024
Complete List of Authors:	Sun, Mengze; Osaka University School of Science Graduate School of Science Department of Physics Otsuka, Yoichi; Osaka University School of Science Graduate School of Science, Frontier Research Center Okada, Maki; Osaka University School of Science Graduate School of Science Department of Physics Shimma, Shuichi; Osaka University School of Engineering Graduate School of Engineering, Department of Biotechnology Toyoda, Michisato; Osaka University, Project Research Center for Fundamental Sciences, Graduate School of Science

SCHOLARONE™ Manuscripts

Data are available upon request from the authors.

### **ARTICLE**

Received 00th January 20xx, Accepted 00th January 20xx

DOI: 10.1039/x0xx000000x

# Probe Oscillation Control in Tapping-mode Scanning Probe Electrospray Ionization for Stabilization of Mass Spectrometry Imaging

Mengze Sun<sup>a</sup>, Yoichi Otsuka \*a,b, Maki Okada<sup>a</sup>, Shuichi Shimma<sup>c</sup> and Michisato Toyoda<sup>a,b</sup>

Mass spectrometry imaging (MSI) is used for visualizing the distribution of components in solid samples, such as biological tissues, and requires a technique to ionize the components from local areas of the sample. Tapping-mode scanning probe electrospray ionization (t-SPESI) uses an oscillating capillary probe to extract components from a local area of a sample with a small volume of solvent and to perform electrospray ionization of those components at high speed. MSI can be conducted by scanning the sample surface with a capillary probe. To ensure stable extraction and ionization for MSI, the probe oscillation during measurements must be understood. In this study, we examined the changes in oscillation amplitude and phase due to the interaction between the oscillating probe and the brain tissue section when the probe tip was dynamically brought close to the sample surface. The changes in the probe oscillation depended on the oscillation frequency and polarity of the bias voltage applied to the solvent because an electrostatic force shifted the frequency of the probe oscillation. These findings suggest that controlling the probe oscillation frequency is important for stabilizing MSI by t-SPESI.

#### 1. Introduction

Mass spectrometry imaging (MSI) has been used to visualize the distribution of various components in solid materials. Biological tissues are among the most common objects to which MSI is applied. Information on the distribution of various molecules, such as metabolites<sup>1,2</sup>, lipids<sup>2–4</sup>, and proteins<sup>5–7</sup>, contained in a tissue section has been reported. MSI requires a technique to ionize molecules in a small area of the tissue. Scanning of the ionization spot is performed to obtain multiple mass spectra related to the sample position. After data acquisition, ion images are obtained by reconstructing the signal intensity of a specific ion in conjunction with the sample coordinates.

Several methods have been developed for ionizing molecules in tissue sections. Secondary ion mass spectrometry (SIMS) $^{8,9}$  is used to ionize samples by irradiating the surface with kiloelectron-volt primary ion beams in an ultra-high vacuum environment. Nanoscale SIMS was developed to provide a higher spatial resolution of up to 50 nm $^{10}$ . However, highenergy primary ion beams can fragment biomolecules, which may limit the information that can be obtained $^{11}$ .

Matrix-assisted laser desorption/ionization<sup>6,12,13</sup> has been used for soft ionization of biomolecules by pulsed laser beams. The tissue section must be pretreated with a matrix to convert

light energy into thermal energy to promote the desorption and ionization of analytes. Because the crystallinity and size of the matrix crystals in the tissue section affect the ionization efficiency, reproducible matrix-coating devices have been used<sup>14</sup>.

Ambient sampling and ionization techniques use a small volume of solvent to extract and ionize molecules under atmospheric pressure. MSI can be conducted rapidly because no matrix deposition on a tissue section is required. Desorption electrospray ionization (DESI) has been widely used<sup>15,16</sup>. Analytes are extracted and ionized by bombarding the sample surface with high-velocity charged solvent droplets, which are generated using a sprayer with a coaxial capillary. Nanospray DESI (Nano-DESI) uses two capillaries arranged in a V-shape<sup>17,18</sup>. One capillary supplies solvent to the sample surface for extraction, and the other is a transfer line for electrospray ionization (ESI) of analytes. Nano-DESI has been used for high-spatial-resolution MSI<sup>19</sup>.

Tapping-mode scanning probe electrospray ionization (t-SPESI) extracts and ionizes molecules in tissue with a vertically oscillating capillary probe<sup>20–23</sup>. The probe oscillation is excited by a piezo actuator attached to the probe, through which a high-voltage solvent is continuously supplied. When the probe is in contact with the sample surface, a liquid bridge is formed between the probe and surface to induce liquid extraction of molecules from the sample. The analytes are subjected to ESI after the probe is retracted from the sample surface. Probe oscillations enable extraction and ionization with sub-picoliter solvent volumes within milliseconds.

To conduct MSI with t-SPESI, the oscillating probe must tap the sample surface appropriately for the extraction and ionization of the sample. To start MSI, the probe positioned

a. Department of Physics, Graduate School of Science, Osaka University, Japan

<sup>&</sup>lt;sup>b.</sup> Forefront Research Center, Graduate School of Science, Osaka University, Japan

<sup>&</sup>lt;sup>c</sup> Department of Bioengineering, Graduate School of Engineering, Osaka University,

Electronic Supplementary Information (ESI) available: [details of any supplementary information available should be included here]. See DOI: 10.1039/x0xx00000x

ARTICLE Analyst

above the sample surface must approach the sample until the probe tip taps the sample surface. In the approach, the probe oscillation will probably be altered by the interaction between the probe tip and the sample surface, but the details have not been investigated. To ensure stable extraction and ionization, we must understand the probe oscillation during the approach.

Previously, we reported the implementation of MSI by adjusting the oscillation frequency of the probe to the resonant frequency. At the resonant frequency, the oscillation energy of the piezo actuator was efficiently used to oscillate the probe, and the probe oscillation amplitude reached its maximum value. This method has been used for many years because of its simplicity in defining the experimental conditions. However, under resonant frequency conditions, a small number of approach failures can occasionally result in missing line scan data, and it is necessary to redo the measurement to obtain perfect MSI data.

In this study, we report the effects of the probe oscillation frequency and solvent bias voltage on the oscillation amplitude and phase during the approach. We developed a new method for measuring the amplitude and phase of oscillations as the distance between the oscillating probe and the sample decreases. The interaction between the probe and mouse brain tissue sections varied with the oscillation frequency of the probe and the polarity of the voltage applied to the solvent. We describe the importance of selecting the oscillation frequency of the probe for stable MSI.

#### 2. Materials and methods

#### 2.1 t-SPESI system

A previously reported t-SPESI system was used <sup>23</sup>. A capillary probe was oscillated using a piezo actuator (PMF-3030, NTK Ceramic, Japan). The PMF-3030 is a small piezo actuator with a diameter of 7.3 mm and length of 17.2 mm, and is capable of providing a maximum displacement of 10  $\mu m$ . The piezo actuator and probe were placed at an angle of 45° to the glass slide surface on which the tissue section was placed. This small actuator was used to prevent the piezo actuator from contacting the sample. A controllable sine-wave voltage signal from the analogue output module (NI 9263, NI, USA) was input into a high-voltage amplifier (M-26110, Mess-Tek, Japan) to drive the piezo actuator. The side of the probe was irradiated by a laser beam (TC20, Neoark, Japan), and the displacement of the shadow of the probe was measured with a segmented photodiode (S5870, Hamamatsu Photonics, Japan) and a custom-made differential amplifier circuit. The output signal of the differential amplifier was input into a lock-in amplifier (LI-5645, NF, Japan) to measure the oscillation amplitude and phase simultaneously. A bias voltage was applied to the solvents via the metal union to which the probe was connected.

The position of the sample was controlled by an XYZ motor stage (a combination of OSMS(CS)-20-35(XY) and OSMS40-5ZF-0B(Z), Sigma Koki, Japan) and a piezo Z-stage (MTKK08S180F30, Mechano Transformer Corporation, Japan). During the approach, the distance between the probe and sample must be

varied significantly, and after the approach, the distance between them must be precisely controlled at a high speed. The motor stage has a large range of motion (5 mm), but the movement speed is slow. On the other hand, the piezo stage has a small range of motion (160  $\mu m$ ) but can move precisely at high speeds. By stacking both stages, the distance between the probe and the sample surface was controlled. For MSI, the gasphase ions generated by t-SPESI were introduced into a quadrupole time-of-flight mass spectrometer (LCMS-9030, Shimadzu, Japan) via a heated ion-transfer tube that formed the path to the mass spectrometer inlet.

#### 2.2 Amplitude/phase vs. distance curve measurement

For the amplitude/phase vs. distance (A/P-D) curve measurements, the piezo Z-stage was moved upward and downward to allow the probe to approach and retract from the sample surface. A triangular wave voltage signal generated by a digital-to-analogue converter (NI 9263, NI) was amplified by a high-voltage amplifier (M-26109, Mess-Tek) and input into the piezo actuator. The input voltage range was 0 to 100 V. The actual displacement of the sample stage was measured using a laser displacement sensor (CDX-L15, OPTEX FA Co., Ltd., Japan) while applying a triangular voltage signal to the piezo stage. The nominal velocity of the piezo stage motion was 37.5  $\mu$ m/s. The hysteresis of the piezo stage motion was calibrated to obtain the piezo displacement vs. voltage curve. (Fig. S1).

A square-wave voltage signal of 10 Hz from a function generator (WF1974, NF) was also used as the start trigger for the stage movement in the X- and Y-directions during the A/P-D curve measurement. The output signals (amplitude and phase) from the lock-in amplifier and the triangular wave voltage signal were recorded simultaneously with a data acquisition device (USB-6343, NI) at 100,000 samples/s while the distance between the probe and sample was changed (Fig. S2). The A/P-D curve measurements were repeated for 12 different points spaced 50  $\mu m$  apart on the same sample.

The position of the probe was monitored from the side using a camera (DN3V-300, Shodensha, Japan) with a macro-zoom lens (MLH-10X, Computar, Japan). Data analysis was performed using a homemade program coded in LabVIEW 2020 (NI).

The A/P-D curve measurements were conducted in two ion modes by changing the polarity of the solvent bias voltage. The solvent was a mixture of *N*,*N*-dimethylformamide and methanol (MeOH; 13024-71 and 21929-81, LCMS grade, Nacalai Tesque, Japan) (1:1 v/v). The solvent flow rate was 20 nL/min, which was controlled using a syringe pump (Legato 185, KD Scientific, USA). The oscillation frequencies were 462.054, 462.524, and 462.984 Hz for the lower than resonant frequency (LRF), resonant frequency (RES), and higher than resonant frequency (HRF) conditions in positive ion mode, respectively. The oscillation frequencies were 462.234, 462.754, and 463.214 Hz for the LRF, RES, and HRF conditions, respectively, in negative ion mode. The volume of solvent consumed in a single extraction-ionization event was estimated to be 0.72 pL by considering the flow rate and oscillation frequencies.

Journal Name ARTICLE

#### 2.3 Capillary probe

A silica tube (I.D. 50  $\mu$ m, O.D. 350  $\mu$ m, Polymicro, Molex Inc., USA) was cut to 50 cm and was cleaned by pumping MeOH (321-00025, Wako Pure Chemical Industries, Japan) through at a flow rate of 0.01 mL/min (LC-20AD, Shimadzu) for over 10 h. The central part (approximately 2 cm) of the 12-cm-long tube was heated using a gas burner to remove the polyimide coating and expose the fused silica tube. A laser puller (P-2000, Sutter Instrument, USA) was used to fabricate capillary probes. The inner diameter of the probe apex was approximately 5  $\mu$ m. The parameter settings for the laser puller are listed in Table S1.

#### 2.4 Sample preparation

Mouse brain (C57, Japan Bio Serum, Japan) sections 8  $\mu$ m thick were prepared by using a cryomicrotome (CM1950, Leica, Germany) and placed on a glass slide (S1126, Matsunami Glass Ind., Ltd., Japan). Tissue sections were frozen at  $-80\,^{\circ}$ C in Falcon tubes containing silica gel (17091-55, Nacalai Tesque). Before the measurement, the tube was returned to room temperature. The quartz substrates ( $20 \times 20 \times 1$  mm, Labo-USQ, Daiko MFG, Japan) were washed with ultrapure water (Direct-Q UV3, Merck, Germany) in an ultrasonic cleaner (ST-01D, Sonictech, Japan) for 10 min, and then dried under a nitrogen gas flow.

#### 2.5 MSI of mouse brain

MSI of the mouse brain section was conducted under three probe oscillation conditions. The solvent was the same as that used for the A/P-D curve measurement. Voltages of 2.5 and -2.5 kV were applied to the solvent for the positive and negative ion mode measurements, respectively. The solvent flow rate was 20 nL/min. To maintain the oscillation amplitude during probe scanning over the sample surface, feedback control was used<sup>24</sup>. Probe scanning was performed with a line spacing of 150 µm for each oscillation frequency condition. The line scan was started on a glass slide approximately 100 µm from the tissue surface. All the line scans had the same length (10 mm). Scanning speed was 1.5 mm/s. The scanning position was shifted by 50 μm to prevent overlap of the probe scanning. In positive ion mode, the oscillation frequencies were 599.372, 599.582, and 599.942 Hz for the LRF, RES, and HRF conditions, and in negative ion mode, they were 545.247, 545.637, and 545.783 Hz, respectively. The volume of solvent consumed in a single extraction-ionization event was estimated to be 0.55 to 0.61 pL by considering the flow rate and oscillation frequencies.

Multiple data files obtained after the series of probe scans were merged and analysed by using IMAGEREVEAL MS (Shimadzu). The ion intensities were normalized by the total ion intensity. The region of the mouse brain was used as the region of interest (ROI). Ion peaks in the range m/z 500–1000 were used. The ion peaks were tentatively assigned for level 2 putative annotation<sup>25</sup> with the results of LIPID MAPS structure searches<sup>26</sup>. As positive ions, proton ([M + H]+), sodium ion ([M + Na]+), and potassium ion ([M + K]+) adducts were the targets, and a mass tolerance of  $\pm 0.005$  was used. For negative ions, deprotonated molecules ([M - H]-) were the targets, and a mass tolerance of  $\pm 0.005$  was used.

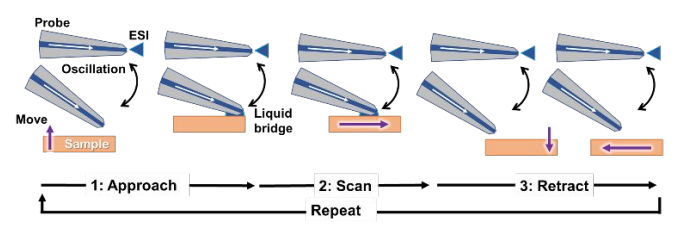


Fig. 1 Schematic of the three steps in MSI with t-SPESI. The distance between the probe tip and sample was controlled before and after probe scanning on the sample surface.

#### 3. Result & Discussion

#### 3.1 Three steps for MSI with t-SPESI

When MSI is conducted using t-SPESI, the following three steps are performed sequentially (Fig. 1).

- 1: Approach. The probe is oscillated vertically, and the solvent flows inside the probe. Moving the sample stage upward reduces the distance between the probe and sample surface continuously. The oscillation amplitude decreases further after the probe tip is in contact with the sample. When the oscillation amplitude reaches a predetermined set-point value, the sample stage stops.
- 2: Scan. The sample stage is moved at a constant speed in one direction (X-direction) relative to the probe. During scanning, the sample components are extracted and ionized, and their gas-phase ions are introduced into the mass spectrometer to obtain mass spectra. In the present study, mass spectra were recorded every 100 ms during probe scanning.
- 3: Retract. After the single-line scanning is completed, the sample is moved downward until the probe tip is not in contact with the sample. The sample position is then moved back to the starting point of the scan (X-direction) and moved to the starting point of the next scan line (Y-direction).

By executing these three steps a predetermined number of times, mass spectra associated with the sample position in the two-dimensional area are obtained. To conduct MSI, the approach in Step 1 must be successful. Owing to the interaction between the probe and the sample, the oscillation amplitude can be changed. We expect that the reproducibility of the approach can be improved by clarifying how the probe oscillation frequency and the polarity of the bias voltage applied to the solvent affect the oscillation amplitude and phase during the approach.

#### 3.2 Probe oscillation in t-SPESI

We previously reported that the relationship between the probe length and resonant frequency can be evaluated by using a cantilever-beam resonance model. The resonant frequency increased linearly with respect to the inverse of the square of the probe length<sup>24</sup>. Thus, we assumed that the probe oscillation in t-SPESI is analogous to the cantilever oscillation in atomic force microscopy. The equation of motion of a resonant cantilever is expressed as

$$m\frac{\partial^2 \Delta z}{\partial t^2} + \frac{m\omega_0 \partial \Delta z}{Q} + m\omega_0^2 \Delta z = F_{ext}$$
 (1)

ARTICLE Analyst

where  $\omega_0$  is the angular frequency of the resonance point of the cantilever in free oscillation, Q is the Q value of the mechanical system of the cantilever, m is the converted mass of the probe oscillation,  $F_{ext}$  is the external force that induces probe oscillation, and Z is the coordinate for the oscillation probe tip. By solving the equation of motion, the oscillation amplitude and phase can be expressed as

$$A = \frac{Q\omega_0^2 A_b}{\sqrt{Q^2 (\omega_0^2 - \omega^2)^2 + \omega_0^2 \omega^2}}$$

$$\phi = \arctan\left[\frac{-\omega/\omega_0}{Q(1-\omega^2/\omega_0^2)}\right]$$
(2)

where  $A_b$  is the oscillation amplitude of the piezoelectric actuator used to oscillate the probe. The relationship between A and frequency is known as the Q-curve. The Q-curve can be regarded as a variant of the Lorentz function<sup>27</sup>. The force between the tip of the probe and sample causes a shift in the resonant frequency  $^{28-30}$  that is expressed as

$$\Delta\omega = \omega_0' - \omega_0 = \omega_0 \frac{k'}{2k} = -\frac{\omega_0 \partial F_{ts}}{2k} |_{z=0}$$
 (4)

where the  $\omega_0$  is the shifted resonant frequency, k is the spring constant due to the probe–sample interaction, and k is the natural spring constant of the probe. Here,  $F_{ext}$  is replaced by  $F_{ts}$ , which includes all the interactions with the probe oscillation, and the zero point corresponds to the equilibrium position of the tip for the oscillation. As an attractive (repulsive) force is formed between the probe and the sample, a negative (positive) shift in resonant frequency occurs. The mismatch between the resonant frequency and probe excitation frequency results in a loss of the resonance condition, and the oscillation amplitude and phase are changed.

In this study, we investigated the changes in the probe oscillation amplitude and phase due to the interaction between the probe and the mouse brain section during the approach step in MSI with t-SPESI.

#### 3.3 Development of the measurement system

To measure the changes in probe oscillation during the approach process, we developed a measurement system to obtain an A/P-D curve. The A/P-D curve indicates the relationship between the probe—sample distance and the oscillation amplitude or phase.

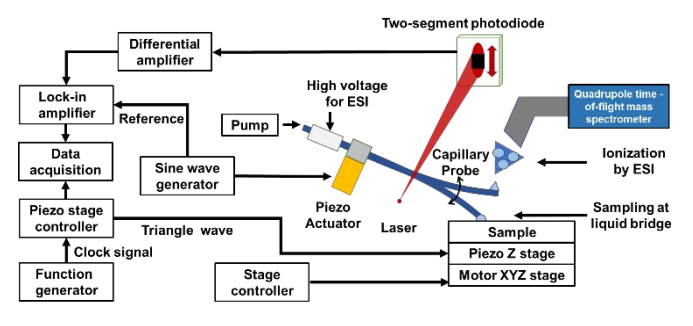


Fig. 2 Block diagram of the t-SPESI system for A/P-D curve measurements. The probe oscillation was controlled by inputting a sine wave voltage signal to the piezo actuator. The side of the probe was irradiated with a laser beam to form a probe shadow. The probe displacement was measured by the voltage difference between the segmented photodiodes. The oscillation amplitude and phase were measured using a lock-in amplifier. The probe oscillation amplitude, phase, and voltage signal input to the piezo Z-stage were recorded simultaneously.

Fig. 2 shows the block diagram of the measurement system. A program for varying the probe—sample distance was implemented in the t-SPESI system reported previously<sup>23</sup>. The distance between the probe and the sample was dynamically changed by supplying a triangular voltage to the piezo Z-stage.

A probe approach was conducted for 12 positions in a single measurement. The voltage signal to the piezo Z-stage, oscillation amplitude, and oscillation phase were recorded simultaneously throughout the measurement. The data were then processed to obtain an averaged A/P-D curve in the following steps.

- 1: Separation of the dataset for each approach step from the time series of oscillation amplitude and phase (Fig. S3).
- 2: Merging of the value of the piezo Z-stage position and the amplitude/phase value to obtain an A/P-D curve (Fig. S4).
- 3: Detection of the Z-stage position where the probe was in contact with the sample surface (Fig. S5).
- 4: Data averaging of multiple A/P-D curves.

# 3.4 Comparison of the A/P-D curves in positive and negative ion mode

The A/P-D curves for the mouse brain section were measured using LRF (462.054 Hz), RES (462.524 Hz), and HRF (462.984 Hz) probe oscillation frequencies. To control the frequency, the phase value measured with the lock-in amplifier was adjusted to  $-70^{\circ}$ ,  $-90^{\circ}$ , and  $-110^{\circ}$  for the LRF, RES, and HRF, respectively.

Figs. 3a and 3b show the amplitude–distance (A-D) curve and the phase–distance (P-D) curve obtained in positive ion mode, respectively. A bias voltage of 2.5 kV was applied to the solvent inside the probe. The zero value on the horizontal axis shows the Z-stage position at which the probe started tapping the mouse brain section. In the A-D curve (Fig. 3a), the amplitude changed differently depending on the oscillation frequency until tapping (distance > 0). The amplitude increased at the LRF, decreased at the HRF, and decreased slightly at the RES with decreasing distance. After tapping (distance < 0), the amplitude decreased for all conditions with decreasing distance, and the degree of linearity in the decrease was

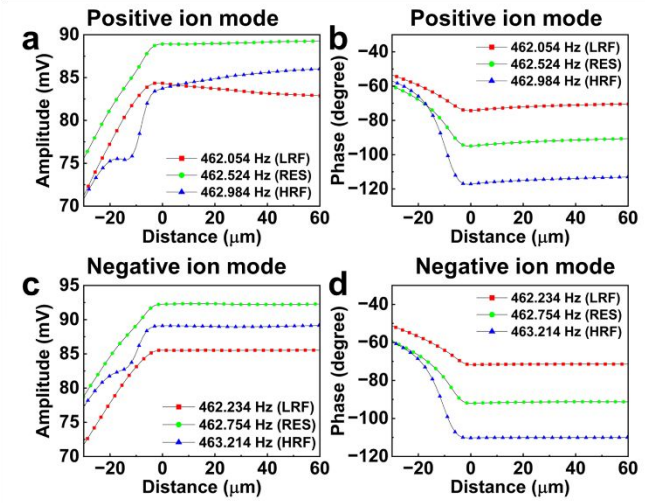


Fig. 3 A/P-D curves in positive ion mode (a, b) and negative ion mode (c, d).

Journal Name ARTICLE

different, especially for the HRF. In the P-D curve (Fig. 3b), the phase values decreased when the probe approached the sample surface until tapping. Similar trends were obtained for all the oscillation frequencies. The phase values increased after the probe tapped the sample surface. The phase increase after tapping was larger when the oscillation frequency was HRF.

The A/P-D curves obtained in negative ion mode are shown in Figs. 3c and 3d, respectively. A bias voltage of -2.5 kV was applied to the solvent. In the A-D curve (Fig. 3c), the amplitude was almost constant until tapping. After tapping, the amplitude decreased for all conditions, such as in positive ion mode, and the degree of linearity of the amplitude decrease was different, particularly for the HRF. In the P-D curve (Fig. 3d), the phase values were constant when the probe approached the sample surface until tapping. Similar trends were observed for all oscillation frequencies. The phase values increased after the probe tapped the sample surface. Similar to the P-D curve in positive ion mode (Fig. 3b), the phase increase after tapping was larger when the oscillation frequency was HRF.

The A/P-D curves with error bars are shown in Fig. S6. The variation in the measurement data is attributed to the variation in the distance between the probe and the sample at each measurement point due to the tilt and unevenness of the sample. Even when considering the error bars, the A/P-D curves were found to vary depending on the oscillation frequencies.

In addition to the measurement of A/P-D curves on mouse brain tissue sections, the A/P-D curves were measured on a quartz substrate. Unlike the measurements on brain tissue sections, positive ion mode measurements did not show large changes in amplitude or phase until tapping. The negative ion mode measurements were similar to those of the brain tissue sections (Fig. S6).

### 3.4.1 Probe-sample interactions until probe tapping

The trends in the A/P-D curves obtained in positive ion mode depended on the oscillation frequency until the probe tapped the sample surface. These changes could be due to the attractive interaction between the probe apex and the sample.

As noted in Section 3.2, the attractive force results in a negative shift in the resonant frequency. The amplitude–frequency relationship is described as a variant of the Lorentz function. Thus, the amplitude should increase when the oscillation frequency is the LRF, owing to the negative shift in the resonant frequency. Conversely, the amplitude should decrease when the oscillation frequency is the RES or HRF. The decrease in amplitude should be larger for the HRF than for the RES. Because the phase–frequency relationship is represented by the arctan function, the phase values would decrease for all oscillation conditions (LRF, RES, and HRS) owing to the negative shift of the resonant frequency.

The attractive interaction is likely caused by the electrostatic force between the negatively charged mouse brain tissue and the positively charged solvent at the probe tip. Previous reports have shown that the cellular membrane has a negative surface charge influenced by the three-dimensional structure of

proteins and the types of amino acids and lipids on the cell membrane  $^{31,32}$ .

The A/P-D curves obtained in negative ion mode showed little change in the oscillation amplitude and phase until tapping. Thus, the electrostatic repulsive force between the negatively charged tissue and the solvent from the probe tip was weak. The reason for the suppression of repulsive force is not yet understood. The results in Fig. 3 suggest that the amount of charge induced on the solvent surface at the probe tip is asymmetric depending on the polarity of the applied voltage. The amount of charge induced at the probe tip may be greater when a positive voltage is applied than when a negative voltage is applied.

#### 3.4.2 Probe-sample interactions after probe tapping

After the probe tapping, the amplitude decreased and the phase increased. During this period, the probe—sample distance decreased, and the repulsive interaction between the tip and sample increased. In other words, the space for probe oscillation decreased, and the value of the positive resonant frequency shift increased simultaneously, explaining the monotonous decrease in amplitude in the A-D plots for the LRF and RES conditions. Because the amplitude—frequency relationship is described as a variant of the Lorentz function, the amplitude decreased after probe tapping owing to the positive shift of the resonant frequency. The decrease in the probesample distance matches the decrease in amplitude.

In contrast, when the oscillation frequency was HRF, the amplitude increased until the positively shifted resonant frequency exceeded the probe oscillation frequency. The amplitude then decreased because the resonant frequency was higher than the oscillation frequency. The shift in the resonant frequency across the oscillation frequency for the HRF condition could result in unique nonlinear amplitude changes during the process after probe tapping. As the probe-sample distance decreased, the oscillation amplitude increased because of the repulsive force. The increase in the amplitude may have increased the repulsive force further and accelerated the positive shift in the resonant frequency. This may be why the amplitude decreased substantially just after the probe tapping under the HRF condition. The subsequent smaller decrease in amplitude may also be due to a larger repulsive force, which caused a smaller amplitude than the probe–sample distance.

In the P-D curves (Figs. 3c and 3d), the phase values increased for all oscillation conditions in both ion modes after probe tapping. When the probe—sample distance was 0 to –20  $\mu m$ , the size of the increase in the phase was in the order LRF < RES < HRF. This result corresponds to the larger phase shift near the resonant frequency (–90° in phase), considering that the phase—frequency relationship is represented by the arctan function.

When the probe taps the sample surface, the formation and breaking of a liquid bridge and the generation of the electrospray of the extractants occur sequentially at the probe tip. The kinetic energy of the probe oscillation is dissipated in each of these processes. However, this paper focuses on the

ARTICLE Analyst

probe approach process, and thus future work is necessary to elucidate the effect of energy dissipation on the sampling and ionization processes.

#### 3.5 Effect of bias voltage on the probe-sample attractive force

Measurements of the A/P-D curves in positive ion mode revealed that attractive electrostatic forces may occur until probe tapping. To investigate the electrostatic force between the probe and the sample associated with the solvent bias voltage, two types of measurements were performed.

First, the oscillation phase value was measured at a constant solvent bias voltage and oscillation frequency. If the electrostatic force between the probe and sample changes in response to the bias voltage, the phase value should decrease. Second, the oscillation frequency was adjusted so that the phase remained constant at a constant solvent bias voltage. A frequency shift would occur if the electrostatic force between the probe and the sample were to change as a function of the bias voltage. In both experiments, the probe was fixed 80  $\mu m$  above the mouse brain tissue section.

Fig. 4a shows the results of the first method in positive ion mode. The oscillation frequency was adjusted to 452.340 Hz (RES condition) when a bias voltage of 2.5 kV was applied. The phase decreased as the bias voltage was increased. In contrast, the phase value remained at approximately –90° irrespective of the bias voltage in the negative bias voltage conditions (Fig. 4b). This result suggests a negative shift in the phase value due to the attractive force between the probe and sample in positive ion mode.

In the second method, the phase was adjusted to  $-70^\circ$ ,  $-90^\circ$ , and  $-110^\circ$  for the LRF, RES, and HRF conditions, respectively. The phase values were adjusted for each bias voltage condition, and the oscillation frequencies were measured. The oscillation frequency decreased for all conditions with increasing positive bias voltages (Fig. 4c).

An obvious resonant frequency shift was not observed under negative bias voltage conditions (Fig. 4d). Thus, there was a negative shift of the resonant frequency in positive ion mode

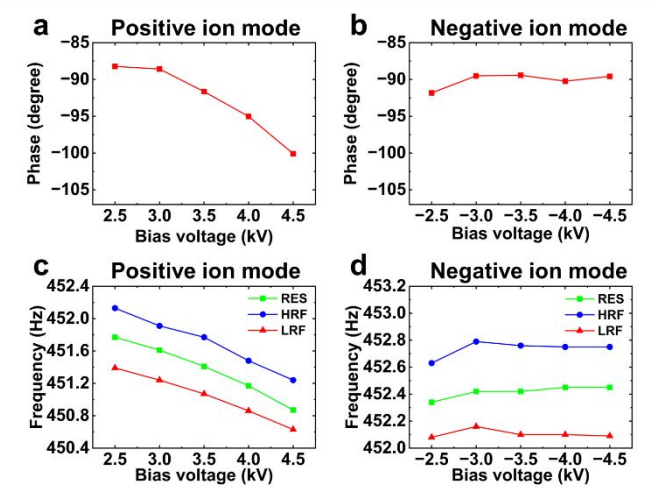


Fig. 4 Relationship between the solvent bias voltage and the oscillation phase in positive ion mode (a) and negative ion mode (b). Relationship between the solvent bias voltage and the oscillation frequency in positive ion mode (c) and negative ion mode (d)

due to the attractive electrostatic interaction between the positively charged solvent at the probe tip and the negatively charged mouse brain tissue.

#### 3.6 MSI of mouse brain sections

In MSI with t-SPESI, the probe approach and probe scanning are repeated multiple times, as described in Section 3.1. The probe approach stops when the amplitude value reaches the predetermined set point value. Ideally, the probe tip must tap the sample when the approach is completed.

Here, we discuss the effect of the probe oscillation frequency and the polarity of the bias voltage applied to the solvent on the MSI of mouse brain sections. MSI was conducted in the positive and negative ion modes. In each mode, measurements were performed with the same sample and probe under three oscillation frequency conditions. The position of the sample was adjusted to prevent the overlap of the probe scanning area for each frequency condition.

Figs. 5a and 5b show the ion images for m/z 782.564 (phosphatidylcholine (PC) 34:1, [M + Na]<sup>+</sup>) and m/z 848.640 (phosphatidylserine (PS) 40:0, [M + H]<sup>+</sup>) acquired in positive ion mode, respectively. When the probe oscillation frequency was the LRF, the distribution of lipids was visualized across the entire brain section, and the distribution depended on the lipid type. However, for the RES condition, several lines of missing data were observed, and for the HRF, little signal was obtained from the tissue. These results show that changes in the oscillation amplitude during the probe approach affect the MSI.

As shown in the analysis of the A/P-D curves, under the LRF condition, the amplitude increased as the probe approached the sample. After probe tapping, the approach continued, the amplitude decreased, and the approach was completed. The probe-sample distance and oscillation amplitude change are inversely correlated; thus, approach failure can be avoided.

In contrast, under the HRF condition, the amplitude decreased as the probe approached the sample. Before the

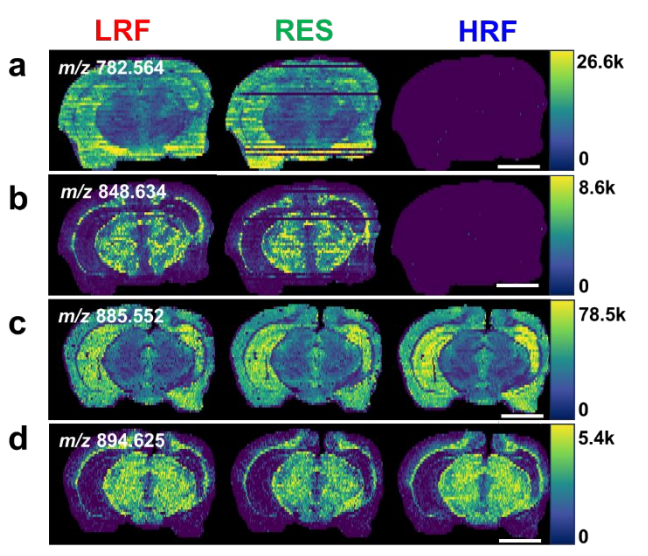


Fig. 5 Ion images of mouse brain sections in positive ion mode for PC 34:1 [M + Na] $^+$  (a) and PS 40:0 [M + H] $^-$  (b) and in negative ion mode for PI 38:4 [M - H] $^-$  (c) and PS 44:4 [M - H] $^-$  (d) with different probe oscillation frequencies. Scale bar: 2.5 mm.

Journal Name ARTICLE

probe tapped the sample, the amplitude reached the set point, and the approach was stopped. Although the probe did not tap the sample, the probe scan began, and no extraction and ionization of the tissue components occurred.

Under the RES condition, although the amplitude decreased slightly during the probe approach, most of the approaches were successful. The approach failed for several probe-scanning lines, suggesting that other factors destabilize probe oscillations during the approach step. In addition to the electrostatic attractive force, instability of the solvent flow could be another factor that changes the oscillation frequency of the probe. If the solvent flow rate increases (decreases) in a short time, the amount of solvent flowing out of the probe tip could increase (decrease), which would decrease (increase) the resonant frequency and possibly decrease the oscillation amplitude. We are currently working on stabilizing the solvent flow and will report the details in a future publication.

Figs. 5c and 5d show the ion images of m/z 885.552 (phosphatidylinositol (PI) 38:4, [M – H]<sup>-</sup>) and m/z 894.625 (PS 44:4, [M – H]<sup>-</sup>) acquired in negative ion mode. The lipid distribution in the whole brain section was visualized for all probe oscillation frequencies, and the distribution depended on the lipid type. This difference in results from positive ion mode MSI was due to the probe oscillation stability during the approach. The oscillation amplitude did not change until the probe tapped the sample, as revealed by the analysis of the A/P-D curves. MSI in negative ion mode showed that the probe approach was stable regardless of the oscillation frequency.

Comparing the ion images obtained by MSI showed that the probe oscillation frequency should be set lower than the resonant frequency to stabilize the probe approach when conducting MSI in positive and negative ion modes.

In this study, the A/P-D curves were measured at a solvent flow rate of 20 nL/min. The realization of a high-spatial-resolution MSI requires a reduction in the volume of the liquid bridge. In the future, nanoflow pumps will be used to achieve stable solvent delivery at low flow rates.

We previously reported that a mixture of DMF and MeOH is appropriate for imaging lipids in mouse brain tissues<sup>23</sup>. Thus, we studied the A/P-D curves using a DMF/MeOH mixture. t-SPESI allows us to change the solvent composition, which can improve the selectivity and/or efficiency of the extraction-ionization of biological molecules. When using solvents with different physicochemical properties, it would be possible to optimize the probe oscillation frequency by measuring the A/P-D curves.

#### 4. Conclusions

We investigated the effects of probe oscillation frequency and solvent bias voltage on the stability of MSI by t-SPESI. We developed a method to measure the relationship between the probe—sample distance and the probe oscillation amplitude/phase. The experimental results showed that the oscillation amplitude and phase depended on the two factors before and after the probe tapped the sample surface. Electrostatic attractive forces were generated between the probe and the mouse brain section in positive ion mode

measurements and the probe oscillation frequency determined whether the approach was successful or unsuccessful. To conduct MSI in the positive and negative ion modes with the same probe, it is important to set the probe oscillation frequency lower than the resonant frequency to stabilize the probe oscillation during the approach. Combining this finding with the t-SPESI measurement system is expected to stabilize the measurement of tissue sections further and improve the MSI throughput.

#### **Author Contributions**

Mengze Sun: Software, methodology, validation, formal analysis, investigation, visualization, data curation, and writing-original draft preparation.

Yoichi Otsuka: Conceptualization, methodology, software, investigation, writing-original draft preparation, writing-review & editing, supervision, project administration, funding acquisition.

Maki Okada: Resources. Shuichi Shimma: Resources.

Michisato Toyoda: Resources, writing – review & editing.

#### **Conflicts of interest**

The authors declare that they have no conflicts of interest.

#### Acknowledgements

The authors are grateful to Dr. Ichii of Kyoto University for fruitful discussions on probe vibration of AFM. This work was supported by the Japan Agency for Medical Research and Development (AMED) under grant numbers JP21he0322005and JP22ym0126815, the Naito Foundation, the Japan Science and Technology Agency (JST), PRESTO Grant Number JPMJPR20E4, Japan Society for the Promotion of Science (JSPS) KAKENHI grant number JP23H03711, Toyota Riken Scholar, and Hyogo Science and Technology Association.

#### References

- N. Morse, T. Jamaspishvili, D. Simon, P. G. Patel, K. Y. M. Ren, J. Wang, R. Oleschuk, M. Kaufmann, R. J. Gooding and D. M. Berman, *Laboratory Investigation*, 2019, 99, 1561–1571.
- A. Ajith, S. Mondal, S. Chattopadhyay, A. Kumar, Y. Sthanikam,
   A. G. Chacko, K. Prabhu, G. Chacko, H. A. Vanjare, R. V. Rajesh
   and S. Banerjee, ACS Chem Neurosci, 2021, 12, 4187–4194.
- 3 A. M. Moerman, M. Visscher, N. Slijkhuis, K. Van Gaalen, B. Heijs, T. Klein, P. C. Burgers, Y. B. De Rijke, H. M. M. Van Beusekom, T. M. Luider, H. J. M. Verhagen, A. F. W. Van der Steen, F. J. H. Gijsen, K. Van der Heiden and G. Van Soest, *J Lipid Res*, 2021, **62**, 100020.
- W. Michno, P. M. Wehrli, S. Koutarapu, C. Marsching, K. Minta, J. Ge, S. W. Meyer, H. Zetterberg, K. Blennow, C. Henkel, J. Oetjen, C. Hopf and J. Hanrieder, *J Neurochem*, 2022, **160**, 482–498.
- 5 H. J. Cooper and O. J. Hale, Anal Chem, 2021, 93, 4619–4627.

60

ARTICLE Analyst

 R. M. Caprioli, T. B. Farmer and J. Gile, *Anal Chem*, 1997, 69, 4751–4760.

- 7 A. M. Kip, J. M. Valverde, M. Altelaar, R. M. A. Heeren, I. H. R. Hundscheid, C. H. C. Dejong, S. W. M. Olde Damink, B. Balluff and K. Lenaerts, *J Proteome Res*, 2022, **21**, 49–66.
- M. M. Lozano, Z. Liu, E. Sunnick, A. Janshoff, K. Kumar and S. G. Boxer, *J Am Chem Soc*, 2013, 135, 5620–5630.
- P. Agüi-Gonzalez, S. Jähne and N. T. N. Phan, J Anal At Spectrom, 2019, 34, 1355–1368.
- 10 D. Oehler and S. Cady, *Challenges*, 2014, **5**, 260–283.
- 11 I. Barut and J. S. Fletcher, Biointerphases, 2023, 18, 061202.
- 12 M. Wang, K. Dubiak, Z. Zhang, P. W. Huber, D. D. Y. Chen and N. J. Dovichi, *Talanta*, 2019, **204**, 138–144.
- 13 L. Qin, Y. Zhang, Y. Liu, H. He, M. Han, Y. Li, M. Zeng and X. Wang, *Phytochemical Analysis*, 2018, 29, 351–364.
- 14 L. Meng, J. Han, J. Chen, X. Wang, X. Huang, H. Liu and Z. Nie, Anal Chem, 2022, 94, 6457–6462.
- 15 Z. Takáts, J. M. Wiseman, B. Gologan and R. G. Cooks, *Science* (1979), 2004, **306**, 471–473.
- 16 Z. Miao, H. Chen, P. Liu and Y. Liu, Anal Chem, 2011, 83, 3994–3997.
- 17 H. J. Cooper and O. J. Hale, Anal Chem, 2021, 93, 4619-4627.
- 18 X. Li, H. Hu, R. Yin, Y. Li, X. Sun, S. K. Dey and J. Laskin, *Anal Chem*, 2022, **94**, 9690–9696.
- 19 R. Yin, K. E. Burnum-Johnson, X. Sun, S. K. Dey and J. Laskin, *Nat Protoc*, 2019, **14**, 3445–3470.
- 20 Y. Otsuka, S. Satoh, J. Naito, M. Kyogaku and H. Hashimoto, *Journal of Mass Spectrometry*, 2015, **50**, 1157–1162.
- 21 Y. Otsuka, S. Shide, J. Naito, M. Kyogaku, H. Hashimoto and R. Arakawa, *Rapid Communications in Mass Spectrometry*, 2012, **26**, 2725–2732.
- 22 Y. Otsuka, J. Naito, S. Satoh, M. Kyogaku, H. Hashimoto and R. Arakawa, *Analyst*, 2014, **139**, 2336–2341.
- 23 Y. Otsuka, N. Ote, M. Sun, S. Shimma, O. Urakawa, S. Yamaguchi, T. Kudo and M. Toyoda, *Analyst*, 2023, **148**, 1275–1284.
- 24 Y. Otsuka, B. Kamihoriuchi, A. Takeuchi, F. Iwata, S. Tortorella and T. Matsumoto, *Anal Chem*, 2021, **93**, 2263–2272.
- 25 L. W. Sumner, A. Amberg, D. Barrett, M. H. Beale, R. Beger, C. A. Daykin, T. W. M. Fan, O. Fiehn, R. Goodacre, J. L. Griffin, T. Hankemeier, N. Hardy, J. Harnly, R. Higashi, J. Kopka, A. N. Lane, J. C. Lindon, P. Marriott, A. W. Nicholls, M. D. Reily, J. J. Thaden and M. R. Viant, *Metabolomics*, 2007, 3, 211–221.
- 26 E. Fahy, S. Subramaniam, R. C. Murphy, M. Nishijima, C. R. H. Raetz, T. Shimizu, F. Spener, G. Van Meer, M. J. O. Wakelam and E. A. Dennis, *J Lipid Res*, 2009, **50**, S9–S14.
- 27 H.-Y. Nie, A. R. Taylor, W. M. Lau and D. F. MacFabe, *Analyst*, 2011, **136**, 2270–2276.
- 28 B. Voigtländer, in Scanning Probe Microscopy: Atomic Force Microscopy and Scanning Tunneling Microscopy, ed. B. Voigtländer, Springer Berlin Heidelberg, Berlin, Heidelberg, 2015, pp. 187–204.
- 29 B. Voigtländer, in Scanning Probe Microscopy: Atomic Force Microscopy and Scanning Tunneling Microscopy, ed. B. Voigtländer, Springer Berlin Heidelberg, Berlin, Heidelberg, 2015, pp. 205–221.
- H. Hölscher and U. D. Schwarz, Int J Non Linear Mech, 2007, 42, 608–625.
- 31 M. Nishino, I. Matsuzaki, F. Y. Musangile, Y. Takahashi, Y. Iwahashi, K. Warigaya, Y. Kinoshita, F. Kojima and S. Murata, *PLoS One*, 2020, **15**, e0236373.

32 S. Eisenberg, E. Haimov, G. F. W. Walpole, J. Plumb, M. M. Kozlov and S. Grinstein, Mol Biol Cell, 2021, 32, 301–310.